Wideband unidirectional transmission with tunable sign-switchable refraction and deflection in nonsymmetric structures

P. Rodríguez-Ulibarri,[1,*] M. Beruete,[1,†] M. Navarro-Cía,[2,3,4,‡] and Andriy E. Serebryannikov[5,§]

[1]*TERALAB (MmW-THz-IR & Plasmonics Laboratory), Universidad Pública de Navarra, Campus Arrosadía, 31006 Pamplona, Spain*

[2]*Optical and Semiconductor Devices Group, Department of Electrical and Electronic Engineering, Imperial College London, London SW7 2BT, UK*

[3]*Centre for Plasmonics and Metamaterials, Imperial College London, London SW7 2AZ, UK*

[4]*Centre for Terahertz Science and Engineering, Imperial College London, London SW7 2AZ, UK*

[5]*Technische Universität Hamburg-Harburg, E-3, D-21071 Hamburg, Germany*

(Received 28 June 2013; revised manuscript received 10 October 2013; published 28 October 2013)

A general theory of reciprocal unidirectional transmission with tunable sign-switchable refraction and deflection of outgoing wave in structures with broken spatial inversion symmetry is presented. Several coupling scenarios connected with the diffraction-inspired asymmetry in transmission are considered for volumetric structures with one-side corrugations. They illustrate conditions of coexistence of diodelike unidirectional transmission and tunability of deflection and refraction, including change of their sign. Simulation results are presented and analyzed for nonsymmetric structures based on the stacked subwavelength hole array metamaterial. It is shown that one-way coupling can appear within a wide range of frequencies and angles of incidence, a part of which may be used to obtain different signs of deflection. Transmission results and field distributions confirm the possibility of obtaining high-contrast unidirectional transmission that can be tuned by varying incidence angle, while frequency is fixed. A pronounced unidirectional transmission is demonstrated at negative deflection in structures that are only $0.47\lambda_0$ thick, whereas a thicker structure is required in order to obtain both signs of deflection in a unidirectional regime.

DOI: 10.1103/PhysRevB.88.165137 PACS number(s): 41.20.Jb, 42.25.Fx, 81.05.Xj, 84.40.−x

I. INTRODUCTION

Asymmetric transmission is known to appear in reciprocal finite-thickness or finite-size structures with broken spatial inversion symmetry, manifesting itself in a strong forward-to-backward transmission contrast. Because of reciprocity, additional transmission channels should be opened for one of the two opposite illumination directions, which can be connected with higher diffraction orders[1–8] or polarization conversion[9–11] and can exploit benefits of inclining interfaces.[12–14] In the first case, asymmetry in transmission is inspired, in fact, by asymmetric diffractions at the opposite interfaces of a grating-like structure. The most interesting regime of asymmetric transmission is probably that with vanishing transmission for one of the two opposite incidence directions, so that unidirectionality takes place. Furthermore, it can be a wideband regime at least if a material or a periodic structure with specific dispersion is utilized to create a nonsymmetric structure.[4,5] Results related to various regimes of the diffraction-inspired asymmetric transmission have recently been reported for photonic crystal gratings,[2,3,5,6] gratings made of ultralow-index materials,[4] and stacked subwavelength hole arrays (SHAs) with one-side corrugations.[15] Moreover, asymmetric transmission can be achieved by using a single nonsymmetric metallic grating with slits,[1,16] or two different metallic gratings with slits and an air gap in between.[17,18]

Metamaterials (MMs), to which SHAs also belong, have been thoroughly analyzed but not yet studied in detail in the context of the diffraction-inspired asymmetric transmission. They are often considered as artificially designed materials that exhibit unusual electromagnetic properties. The most evident example is the achievement of a material with negative index of refraction that was theoretically investigated by Veselago[19] and experimentally demonstrated by Smith *et al.* 30 years later.[20] Unlike most natural materials where propagation is right-handed (RH, positive refraction), properly designed SHAs behave as left-handed (LH) materials; i.e., they show negative index of refraction.[21,22] Another mechanism of negative and zero refraction is well known, which is connected with umklapp scattering at the interfaces rather than with intrinsic properties.[23,24] On the other hand, variation of the incidence angle θ is itself a simple but efficient tool to tune electromagnetic response of various structures; e.g., see Refs. 25–27. In particular, it has been exploited in infinite square-lattice phononic crystals with equifrequency dispersion contours (EFCs) located around the M point, in which sign of refraction can be tuned by varying θ.[26]

In this paper, we study unidirectional transmission with tunable deflection angle of the outgoing wave and switchable sign of refraction and deflection. It is achieved by modifying the coupling scenario at one of the interfaces of a finite-thickness structure due to variation of angle of incidence. We will demonstrate the conditions at which unidirectional transmission and angular tunability of deflection may coexist, and estimate the ranges of tunability in some typical cases. In contrast with Refs. 15 and 26, we focus here on the cases when variation in θ can affect the sign of refraction and deflection of higher order beams, which should be coupled at the corrugated input interface and not coupled at the noncorrugated interface, in order to obtain unidirectional transmission. The paper is organized as follows. In Sec. II, we present a general approach that allows one to detect when the desired combination of unidirectionality and tunability can be obtained. It can be done by assuming general and simple dispersion features and conditions. In Sec. III, we analyze dispersion-relevant results

for SHAs with selected parameters, on which suggested compact finite-thickness structures for unidirectional transmission will be based. In Sec. IV, transmission and contrast maps and field distributions are discussed. A brief conclusion is given in Sec. V.

II. RANGE OF TUNABILITY: DISPERSION-BASED APPROACH

In this section, we obtain general conditions at which tunable unidirectional transmission can be realized. It is known that in the diffraction-inspired unidirectional transmission, zero order must be uncoupled, while one or several higher orders are coupled in a one-way manner, e.g., owing to one-side corrugations.[4,5] Without loss of generality, a infinite structure is considered here (referred to generically as the host structure or host material), which is characterized by circular EFCs; it is assumed that the corrugations can be placed at one of the sides of a finite-thickness slab of a host material, in order to enable the diffraction-inspired asymmetric transmission.[28] Figure 1 shows a schematic diagram of the slab of host material with a grating placed at one of the interfaces. The important quantities involved throughout this paper are highlighted. In line with the grating theory,[29] the mth-order diffraction angle, which is also called the deflection angle in transmission, is determined as

$$\sin\phi_m = \sin\theta + m\Delta_k/k, \tag{1}$$

where $\Delta_k = 2\pi/L$ is the distance between the construction lines, L is the grating period, and $k = \omega/c$ is the wave number. In Eq. (1), ϕ_m is assumed to be measured in the counterclockwise direction with respect to the normal to the exit interface, while θ is measured in the counterclockwise direction with respect to the normal to the incidence interface, as shown in Fig. 1. Restriction to circular EFCs is possible because the width and location of EFCs are important for the studied mechanism rather than their actual shape, which may be, for example, close to elliptical. Therefore, the following discussion will be valid universally, as we will demonstrate afterwards for a hybrid structure or material with noncircular EFCs. Furthermore, since the plane-wave framework is utilized, the analysis presented here is valid for both RH and LH cases. Consideration is restricted here to the case in which EFCs are located around the ($k_y = 0$, $k_z = 0$) point in **k** space.[30]

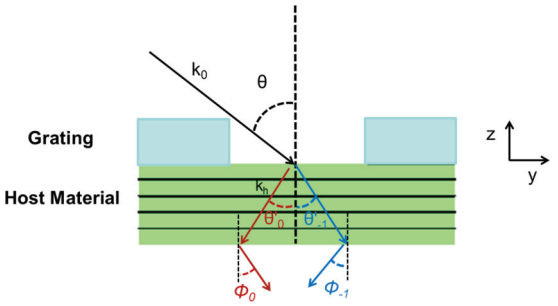

FIG. 1. (Color online) Schematic diagram of the slab of host material stacked with the dielectric grating; $\mathbf{k_0}$ is the free-space wave vector, θ is the incidence angle, θ_0' and θ_{-1}' are the refraction angles for diffraction orders $m = 0$ and $m = -1$, respectively, $\mathbf{k_h}$ is the wave vector in the host material, and ϕ_0 and ϕ_{-1} are the deflection angles for orders $m = 0$ and $m = -1$, respectively. The host material is assumed here to be a LH material. Both diffraction orders are assumed to be propagating in surrounding air and coupled to the waves that may propagate in the host material. Order $m = -1$ is positively refracted at the upper interface leading to negative deflection of the outgoing wave. Order $m = 0$ is negatively refracted leading to positive deflection.

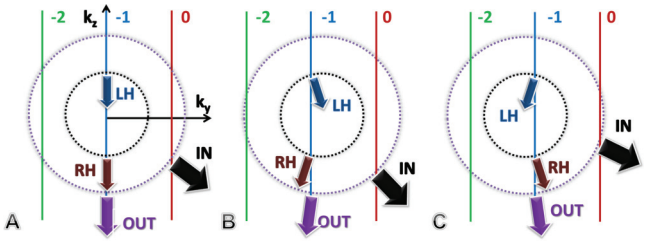

FIG. 2. (Color online) General idea of tunable unidirectional transmission. Larger and smaller circles represent EFCs plotted in the (k_y,k_z) plane for air and host material, respectively. Straight solid lines are construction lines for orders $m = -2$, -1, and 0. Arrows indicated by "IN" and "OUT" schematically show directions of incident and outgoing waves. Arrows indicated by "LH" and "RH" do so for the refracted beams at the corrugated input interface in case of left-handedness and right-handedness. Cases A, B, and C correspond to normally propagating and negatively and positively deflected outgoing waves, respectively.

Figure 2 illustrates the general idea of unidirectional transmission with tunable refraction and deflection. The EFCs for the host material and air are schematically shown together with the construction lines corresponding to zero order and higher orders, which are assumed to be propagating in air only due to one-side corrugations. When an EFC in the material is narrower than in air,[31] an incidence angle can be found where zero order is not coupled to the wave(s) that may propagate inside the host material. Then, there is no transmission when illuminating the noncorrugated side. On the contrary, the order $m = -1$ may propagate and, thus, may be coupled when the corrugated side is illuminated. Hence, unidirectional transmission is expected to appear similarly to some of the structures and regimes studied in Refs. 4,5, and 15. Shifting construction lines in Fig. 2, or, in other words, changing θ, one can obtain zero (case A), negative (case B), or positive (case C) deflection of the single outgoing wave. According to Fig. 2, both negative and positive refraction at the corrugated input interface can correspond to negative deflection ($k_y < 0$), for the cases of RH and LH propagation, respectively (see Fig. 1). These cases have counterparts for positive deflection ($k_y > 0$). For the used shape and location of EFCs, signs of refraction at the corrugated interface and deflection of the outgoing wave are changed simultaneously.

Now let us consider several possible examples for three values of k_h/k_0, where k_h and k_0 mean wave numbers in the host material and free space, respectively. Figure 3 presents three examples of coupling scenarios for $\Delta_k > 2k_h$. In Fig. 3(a), the limiting case is shown when $\Delta_k = k_h + k_0$. Here, the order $m = -1$ is not coupled over the entire range of k_y variation. Taking a smaller value of Δ_k, i.e., $2k_h < \Delta_k < k_h + k_0$, one can obtain a narrow range of k_y variation, in which the order $m = -1$ is coupled to the wave

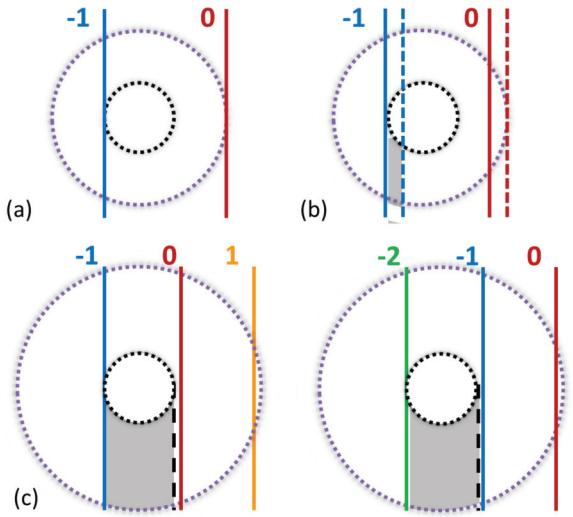

FIG. 3. (Color online) Coupling scenarios at $\Delta_k > 2k_h$. (a) $\Delta_k = k_h + k_0$, (b) $2k_h < \Delta_k \leqslant k_h + k_0$, solid and dashed lines corresponding to two different angles of incidence, and (c) $2k_h < \Delta_k \leqslant -k_h + k_0$ for two different angle incidence scenarios. EFCs are shown in the (k_y, k_z) plane. Construction lines are shown for $m = -2$, -1, 0, and 1. The shadowed area covers the k_y range, for which one-way coupling can appear.

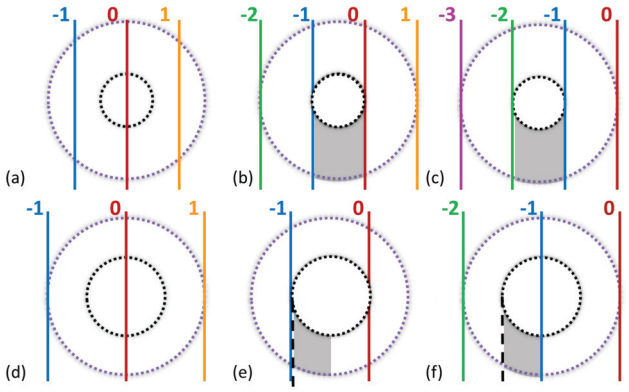

FIG. 4. (Color online) Coupling scenarios at $\Delta_k = 2k_h$. (a)–(c) $k_h = k_0/3$; (d)–(f) $k_h = k_0/2$. EFCs are shown in the (k_y,k_z) plane. Construction lines are shown for $m = -3$, -2, -1, 0, and 1. The shadowed area covers the k_y range, for which one-way coupling can appear.

that propagates in the host material and, thus, unidirectional transmission is possible; see Fig. 3(b). It is seen that ϕ_{-1} can vary in this regime from $\Phi_{\min} = -\arcsin(k_h/k_0)$ rad to $\Phi_{\max} = -\arcsin[(k_h + k_0 - \Delta_k)/k_0]$ rad, and, thus, the entire range of ϕ_{-1} corresponds to negative deflection. Then, the width of the unidirectionality range is given (in units of k_y) by

$$K^{\mathrm{UD}} = k_0 + k_h - \Delta_k. \tag{2}$$

In turn, θ is varied in this case from $\theta_{\min} = \arcsin[(\Delta_k - k_h)/k_0]$ rad to $\theta_{\max} = \pi/2$.

In order to obtain the entire range of refraction angles, i.e., from $-\pi/2$ to $\pi/2$, while the order $m = -1$ is only coupled, the EFC widths for air and host material must satisfy

$$2k_h < \Delta_k < k_0 - k_h. \tag{3}$$

In other words, it is necessary that $k_0 \geqslant 3k_h$. This situation is demonstrated in Fig. 3(c). In this case, ϕ_{-1} is varied from $\Phi_{\min} = -\arcsin(k_h/k_0)$ rad to $\Phi_{\max} = \arcsin(k_h/k_0)$ rad. Accordingly, $K^{\mathrm{UD}} = 2k_h$.

Let us consider two special cases with $\Delta_k = 2k_h$, which would help to understand the conditions of the simultaneous appearance of unidirectionality and switching between positive and negative deflection. The case of $k_h = k_0/3$ is demonstrated in Figs. 4(a)–4(c). Now, ϕ_{-1} varies from $\Phi_{\min} = -\arcsin(1/3)$ rad to $\Phi_{\max} = \arcsin(1/3)$ rad, while the "refraction" angle at the corrugated interface for the order $m = -1$, $\theta' = \theta'_{-1}$, runs over all possible values once θ and, hence, k_y is varied. Correspondingly, the positive and the negative (in terms of ϕ_{-1} and k_y) deflection ranges show the same width and $K^{\mathrm{UD}} = 2k_h$.

Figures 4(d)–4(f) correspond to the case when $k_h = k_0/2$. Now, θ'_{-1} is varied from $-\pi/2$ to 0; i.e., if coupling occurs owing to the order $m = -1$, refraction is *always* negative. In turn, switching between negative and positive deflection cannot be obtained, although unidirectional transmission may appear. ϕ_{-1} runs in this case from $\Phi_{\min} = -\arcsin(1/2)$ rad to $\Phi_{\max} = 0$ and, thus, $K^{\mathrm{UD}} = k_h$.

If we take $k_0 > 3k_h$, both orders $m = -1$ and $m = -2$ should be coupled and furthermore, $\mathrm{sgn}\phi_{-1} \neq \mathrm{sgn}\phi_{-2}$. Then, the idea of the sign-switchable deflection might lose sense. To ensure that this situation is avoided, one should take $k_0 \leqslant 3k_h$. This would provide the exclusive contribution of the order $m = -1$ to unidirectional transmission.

From the above presented consideration, it follows that the condition of switching sign of deflection and that of the entire-range refraction angle in single-beam unidirectional regime are given by

$$k_h < k_0/2 \tag{4}$$

and

$$k_h = k_0/3, \tag{5}$$

respectively. It is worth noting that the general condition of unidirectional transmission for EFCs located around the ($k_y = 0, k_z = 0$) point, as in Figs. 2–4, $k_h < k_0$ (see Refs. 4,5), is less strong than Eqs. (4) and (5). Thus, Eq. (4) can be used as the necessary condition of the *simultaneous* appearance of unidirectionality and deflection sign switching, while Eq. (5) ensures that the ranges of negative and positive deflection angle have the same width in a single-beam regime. In Table I, the main cases of the aforementioned coupling scenarios are summarized. Situations involving not coupling at all, unidirectionality but not tunability from negative to positive

TABLE I. Table summarizing limiting scenarios of coupling.

Δ_k	k_h	K^{UD}	Deflection
$k_h + k_0$	$< k_0$		
$2k_h$	$k_0/2$	$k_h + k_0 - \Delta_k$	negative
$2k_h$	$k_0/3$	$2k_h$	negative/positive

deflection, and unidirectionality plus switching capability from negative to positive deflection are shown, consequently.

III. TUNABILITY IN STACKED HOLE ARRAYS

The theory presented in Sec. II can be applied for a wide class of materials and structures including those studied in Refs. 2–8, and 15. Among them, SHAs are perfect candidates to be used for demonstration of tunability of unidirectional transmission, since they can lead to quite compact (thin) performances. Depending on the axial period d_z, modes of different nature can be excited, which are associated with either Fabry-Perot resonances that support RH propagation or ET resonances that lead to LH propagation.[32] Note that LH behavior is typical for subwavelength periods d_z.[22] Hence, more compact structures for diffraction-inspired unidirectional transmission can be obtained compared to using SHAs with RH behavior (which corresponds to larger d_z) and, also, to gratings based on photonic crystals[2,5] and ultralow-index media,[4] whereas the dispersion-relevant mechanism of directional selectivity still works. In the case studied in detail in this paper, d_z is small compared to the wavelength and, thus, the first band can be completely related to extraordinary transmission (ET) and LH behavior. Under these conditions SHAs behave as cutoff indefinite media,[33,34] being in agreement with requirements for unidirectional transmission. For this reason and also for better connection with the previous studies, we further focus on the infinite SHA from Ref. 34 and the corresponding finite-thickness structure, in which the broken spatial inversion symmetry required for asymmetric transmission is achieved by adding a dielectric grating at one of SHA's interfaces. In that way, ET resonances and diffraction effects provided by the grating are properly combined in order to couple the desired orders to a Floquet-Bloch (FB) wave propagating inside the SHA and keep zero order totally uncoupled at both illumination sides.

A schematic of the unit cell of the whole structure is shown in Fig. 5. It consists of a finite number of hole array plates (N), which are made of copper (conductivity $\sigma = 5.8 \times 10^7$ S/m), with the structural parameters shown in the caption of Fig. 5. The resulting structure has a total thickness of $D = Nt + (N+1)h + a_z$. The chosen SHA performance is expected to allow us to obtain single-beam unidirectional transmission in a wide ranges of frequencies and incidence angles, according to the general theory of Sec. II. In order to obtain transmission results and field distributions of this structure, the commercial full-wave numerical solver CST Microwave Studio has been used. Figure 5 represents the unit cell of an infinitely replicated structure along x and y axes. The unit cell boundary conditions allow us to consider oblique plane wave incidence in terms of diffraction orders. The structure is assumed to be illuminated with p-polarized waves, i.e., having magnetic field oriented in the x direction. For this structure, zero order can be uncoupled while the order $m = -1$ is coupled at the corrugated-side incidence only, in a wide frequency range.

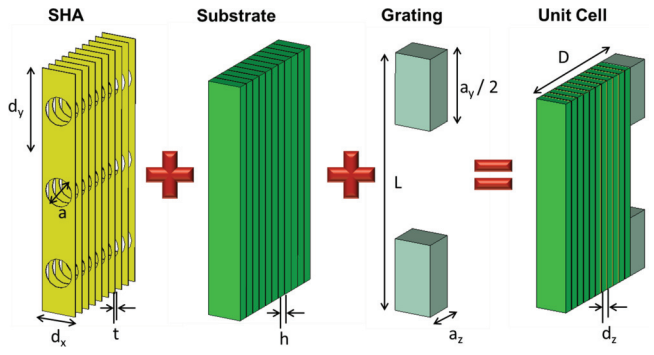

FIG. 5. (Color online) Schematic of SHA + dielectric grating structure. SHA parameters: In-plane period dimensions, $d_x = 1.5$ mm and $d_y = 3.4$ mm; copper thickness, $t = 35$ μm; substrate permittivity, $\varepsilon_s = 2.43$; substrate thickness, $h = 0.49$ mm; axial period, $d_z = 0.525$ mm. Dielectric grating paremeters: Bar thickness, $a_z = 1.27$ mm; bar height $a_y = 5.68$ mm; substrate permittivity, $\varepsilon_g = 10.2$; grating period, $L = 3d_y$.

To illustrate the possibility of tunable operation, Fig. 6 presents EFCs for the lowest FB mode, together with isolines for the values of θ, at which coupling is possible at a given frequency, $\theta = \theta_{\text{in},m}$, where $m = 0, -1$. They are calculated as follows:

$$\theta_{\text{in},m} = \arcsin\left[k_y^{'(m)}/k_0\right] = \arcsin\left[ck_y^{'(m)}/2\pi f\right], \qquad (6)$$

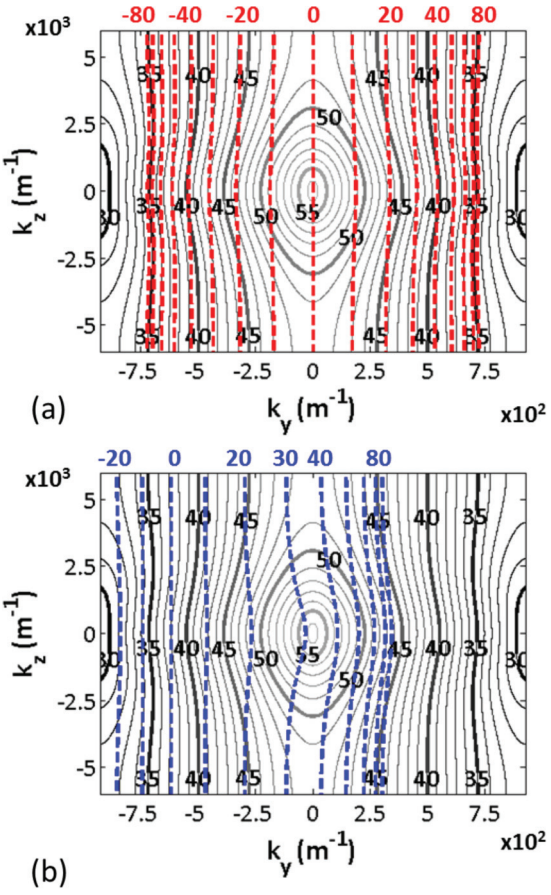

FIG. 6. (Color online) EFCs (solid lines) for the lowest FB mode and isolines (dashed lines) in the (k_y,k_z) plane for $\theta_{\text{in},0}$ in plot (a) and $\theta_{\text{in},-1}$ in plot (b). Numbers near EFCs show frequency in GHz; numbers at the top show the angle value in degrees (step size of 10 degrees between isolines). $k_y = k_y^{(m)}$ with $m = 0$ (a) and $m = -1$ (b).

where $k_y^{'(m)}$ is the tangent wave number for the wave incident on the dielectric grating. $k_y^{(m)}$ is the tangent wave number of the m-order relevant wave inside the host material, here the SHA, and is related to $k_y^{'(m)}$ as

$$k_y^{'(m)} = k_y^{(m)} - \frac{2\pi m}{L}, \tag{7}$$

where $L = 3d_y$ corresponds to the periodicity of the dielectric grating. As is easily observed, what we are doing here is to calculate the angle of incidence (from air) that excites diffraction order m due to the grating and then can couple through the host SHA. Particularizing for $m = 0$ and $m = -1$, the input angle for those orders at the grating interface can be calculated as follows:

$$\theta_{\text{in},0} = \arcsin\left[k_y^{'(0)}/k_0\right] = \arcsin\left[ck_y^{'(0)}/2\pi f\right] \tag{8}$$

and

$$\theta_{\text{in},-1} = \arcsin\left[k_y^{'(-1)}/k_0\right] = \arcsin\left[ck_y^{'(-1)}/2\pi f\right]. \tag{9}$$

So, for an arbitrary pair of $k_y^{(m)}$ and frequency f, there is only one solution for the incident angle. And given the shape of the EFCs (which are clearly anisotropic), the iso-angle contours are not straight lines; see Fig. 6. Using the presented results, one can indicate a simple way to detect whether the orders $m = 0, -1$ are coupled to the FB mode at given f and k_y (or θ), and directly see sign of deflection of the outgoing wave. For example, according to Fig. 6(a), the absence of coupling of zero order at $|\theta| > 20^\circ$ is ensured at $50 < f < 55$ GHz. At the same time, coupling of the order $m = -1$ at $50 < f < 55$ GHz is expected to occur nearly at $25^\circ < \theta < 52^\circ$; see Fig. 6(b). As a result, unidirectional transmission should be possible in rather wide ranges of variation in f and θ. Furthermore, one can see that for a fixed value of f, variation in θ can lead to a change of $\text{sgn}k_y$. Hence, unidirectional transmission and tunability with changeable sign of deflection, both being inspired by diffraction, coexist in the studied SHA. Note that the case of $\phi_{-1} < 0$ ($k_y < 0$) corresponds to the refraction angle $\theta'_{-1} > 0$ (mimicking positive refraction at the corrugated interface), while $\phi_{-1} > 0$ ($k_y > 0$) does to $\theta'_{-1} < 0$ (negative refraction), as a consequence of that $\mathbf{S} \cdot \mathbf{k}_{\text{FB}} < 0$ ($\mathbf{S}$ is the Poynting vetor; $\mathbf{k}_{\text{FB}}$ is the wave vector of the FB mode) in the considered SHA. The tunable sign of ϕ_{-1} can also be obtained when $\text{sgn}\phi_{-1} = \text{sgn}\theta'_{-1}$ that corresponds to the modes with $\mathbf{S} \cdot \mathbf{k}_{\text{FB}} > 0$; see Sec. II.

Figure 7 shows the isolines for ϕ_m, $m = 0, -1, -2$, which are obtained by processing results presented in Fig. 6 and similar results for $m = -2$. The observed features are directly related to the changes in coupling conditions at varying the f-θ set. Three regions filled with isolines for different m are shown. The unidirectional transmission regime involves an f-θ area where zero-order coupling is vanishing and $m = -1$ and $m = -2$ orders are not coupled when impinging from the noncorrugated side. The areas where the isolines are only presented for $m = -1$ or for $m = -2$ correspond to single-beam unidirectional transmission. The former is more interesting because it is expected to show a wider range of tunability in terms of θ and ϕ_{-1} and give the possibility to change sign of ϕ_m. In terms of θ, the range of coupling and tunability at continuous variation in θ for $m = -1$ is

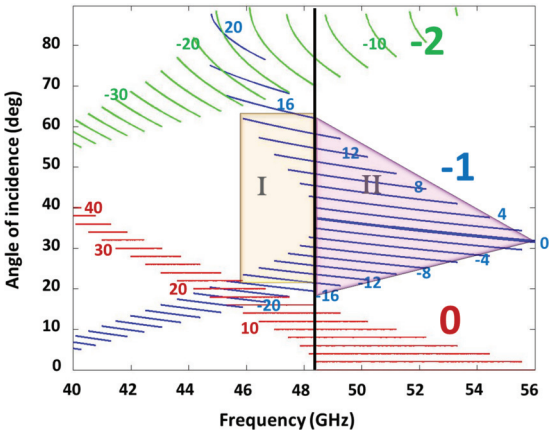

FIG. 7. (Color online) Isolines for ϕ_0, ϕ_{-1}, and ϕ_{-2} (degrees) in (f, θ) plane within the area where coupling to the lowest FB wave is possible. For region I, different signs of ϕ_{-1} can be obtained for two discrete values of θ. In region II tunability and $\text{sgn}\phi_{-1}$ switching can be obtained by a continuous sweep in θ. Solid vertical line is the boundary between the regions where continuous (II) and discrete (I) variation of θ can be used. m is shown by large numbers $(-2, -1, 0)$ for the corresponding group of isolines.

widest at $f \approx 48.4$ GHz (at the left boundary of region II in Fig. 7), with the width $\Delta\theta \approx 38^\circ$ and a deflection angle range of $\Delta\phi_{-1} \approx 32^\circ$. Note that the vicinity of $f = 50$ GHz looks most preferable from the point of view of switching between positive and negative deflection. The isoline for $\phi_{-1} = 0$ sets the boundary between positive and negative deflection, as well as between negative and positive refraction. This case corresponds to a finite-thickness SHA with one-side corrugations considered in Refs. 15.

If just two specific values of ϕ_{-1} that differ in sign are needed rather than the range of continuous variation of ϕ_{-1}, one can use the range $46 < f < 48.4$ GHz (region I in Fig. 7). For example, $\phi_{-1} = -16^\circ$ and $\phi_{-1} = 16^\circ$ are expected to be obtained in the vicinity of $f = 47$ GHz at $\theta = 20^\circ$ and $\theta = 60^\circ$, respectively.

IV. TRANSMISSION RESULTS

Figure 8 presents the maps of the forward (corrugated-side illumination) and backward (noncorrugated-side illumination) transmittances and forward-to-backward transmittance contrast, $T^{\rightarrow}$, $T^{\leftarrow}$ and $\Theta = T^{\rightarrow}/T^{\leftarrow}$, respectively, in the (f,θ) plane, when the number of stacked arrays is $N = 4$ and $N = 10$. On the one hand, a larger N is preferable in order to ensure that the periodic arrangement of hole arrays and relevant dispersion of the FB mode exert the dominant effect on transmission. On the other hand, obtaining of more compact performances remains one of our main goals. For the studied structures, $D/\lambda_0 \approx 0.64$ at $N = 4$ and $D/\lambda_0 \approx 1.17$ at $N = 10$ when $f = 50$ GHz, where λ_0 is the free-space wavelength. To compare, typical performances of nonsymmetric photonic crystal gratings that enable the diffraction relevant asymmetric transmission are typically $2\lambda_0$ to $6\lambda_0$ thick.[5] The boundary between the areas of strong and weak transmission in Figs. 8(a), 8(b), 8(d), and 8(e) coincides well with the boundary of the range of coupling in Fig. 7.

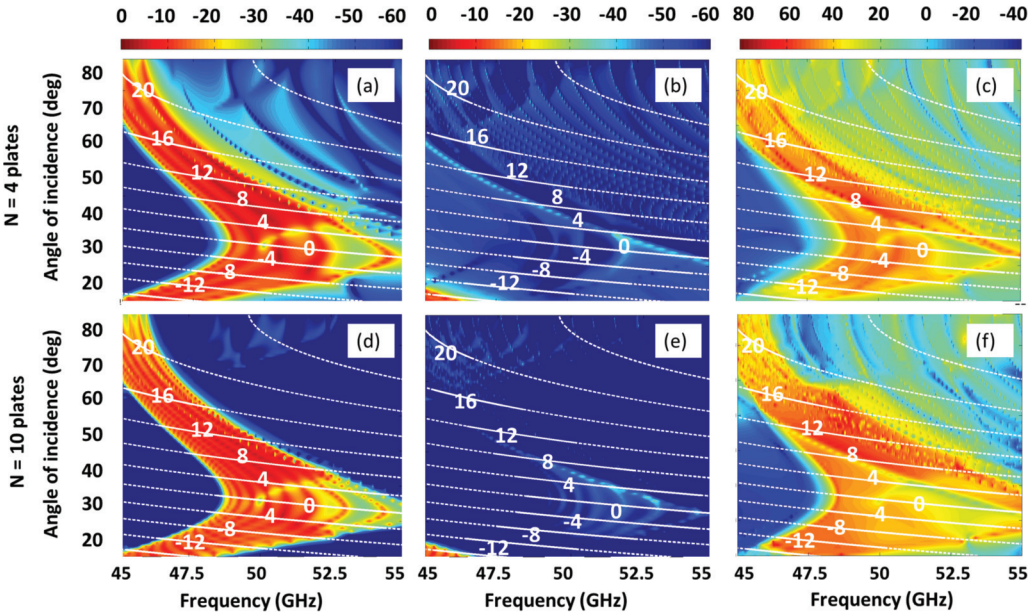

FIG. 8. (Color online) Maps of the forward [(a), (d)] and backward [(b), (e)] transmittance and forward-to-backward transmittance contrast [(c), (f)] in the (f, θ) plane in dB scale. $N = 4$ [(a)–(c)] and $N = 10$ [(d)–(f)]. Solid lines, isolines for ϕ_{-1} from Fig. 7; dashed lines, isolines for ϕ_{-1} obtained from Eq. (1); numbers near isolines, values of ϕ_{-1} in degrees.

Comparing Fig. 8(a) with Fig. 8(b) and Fig. 8(d) with Fig. 8(e), one can see that a wideband unidirectional transmission takes place. Surprisingly, the ranges of variation in f and θ, in which single-beam unidirectional transmission appears due to the order $m = -1$, are even wider than has been expected based on the dispersion results; see Fig. 7. This occurs owing to a very weak coupling of the order $m = -2$ at large θ.

At $N = 4$, the SHA with one-side corrugations is exactly the same as that studied in Ref. 15 in the case of zero deflection. The use of a wide range of parameter variation enables tunable refraction and deflection, which are associated with continuous and discrete variation in θ. In Figs. 8(a) and 8(b) no significant difference is seen as compared to Figs. 8(d) and 8(e), respectively, except for blurring the boundary between the areas, in which strong and weak transmission appear.

The contrast $\Theta = T^{\rightarrow}/T^{\leftarrow}$ is presented in Figs. 8(c) and 8(f) for $N = 4$ and $N = 10$, respectively. It is seen that Θ reaches 60 dB in certain areas in both N plates cases. At $f = 50$ GHz, $\Theta > 35$ dB while θ is varied from 22° to 50° for both $N = 4$ and $N = 10$ cases.

Figure 9 presents the field distribution for unidirectional transmission at $N = 10$ for two different θ causing deflections of opposite sign. It corresponds to the region I in Fig. 7. At the corrugated-side illumination, change of $\mathrm{sgn}\phi_{-1}$ with $\Delta\phi_{-1} \approx 30°$ takes place when a 40° change in θ is applied. In line with the above presented results, transmission at the noncorrugated-side illumination is blocked; see Figs. 9(b) and 9(d). Only several SHAs' axial periods, which are adjacent to the illuminated interface, are strongly affected here by the incident wave. At $\theta = 20°$, umklapp scattering relevant negative deflection seen in Fig. 9(a) coexists with positive refraction at the corrugated incidence interface. In turn, at $\theta = 60°$ [Fig. 9(c)], positive deflection coexists with negative refraction. Figure 10 presents the field distribution that corresponds, in particular, to the region II in Fig. 7, where tunability at continuous variation in θ is possible. Varying θ just by 6°, we obtain $\Delta\phi_{-1} = 5°$. Self-imaging of the field arising after transmission through or reflection from a periodic structure, which is known as the Talbot effect,[35] is pronounced

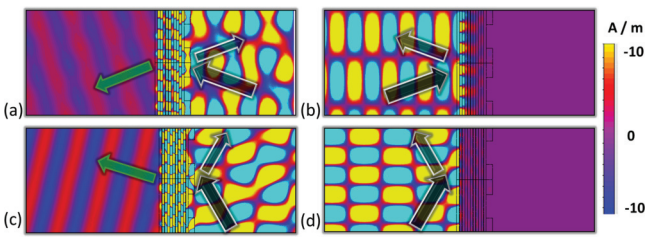

FIG. 9. (Color online) x component of magnetic field at $f = 47$ GHz, (a), (b) $\theta = 20°$, (c), (d) $\theta = 60°$, for $N = 10$; forward [(a), (c)] and backward [(b), (d)] transmission. Greater semitransparent black arrow represents the impinging wave direction. Smaller semitransparent black arrow corresponds to the reflected wave direction. Green arrow stands for the transmitted wave direction. Two grating periods can be observed over the plot height.

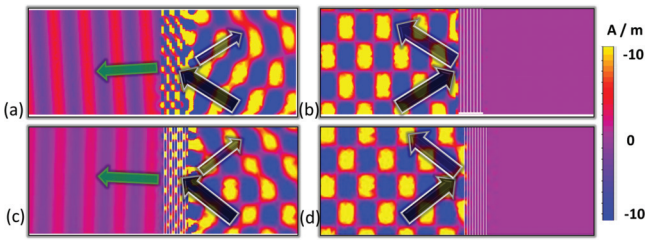

FIG. 10. (Color online) Same as Fig. 9 but for $f = 50$ GHz at (a), (b) $\theta = 32°$, (c), (d) $\theta = 38°$.

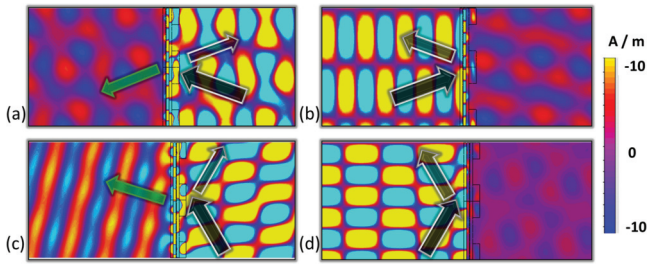

FIG. 11. (Color online) x component of magnetic field at $f =$ 47 GHz, (a), (b) $\theta = 20^\circ$, (c), (d) $\theta = 60^\circ$, for $N = 2$; forward [(a), (c)] and backward [(b), (d)] transmission. Greater semitransparent solid black arrow represents the impinging wave direction. Smaller semitransparent black arrow corresponds to the reflected wave direction. Green arrow stands for the transmitted wave direction. Two grating periods can be observed over the plot height.

at the noncorrugated-side illumination. As seen in Figs. 9 and 10, its manifestations strongly depend on θ.

For comparison, let us consider the case of $N = 2$. Figures 11 and 12 present field distribution when all parameters, except of N, are the same as in Figs. 9 and 10, respectively. Now $D/\lambda_0 \approx 0.47$ at $f = 50$ GHz; i.e., the entire structure is subwavelength. In Fig. 11(c) it can be seen that positive deflection is nicely achieved when impinging from the corrugated side, whereas transmission efficiency for a negatively deflected wave is low. Note that at a slightly larger θ, the order $m = -2$ may be coupled, according to Fig. 7, but this coupling is weak at least at rather large N, as seen in Fig. 8. On the other hand, in such a thin structure the order $m = 0$ is no longer perfectly uncoupled and its coexistence with the order $m = -1$ may deprecate the negative deflection response; see Fig. 11(a). Focusing now on Figs. 12(a) and 12(b), one can see that a pronounced asymmetry in transmission can occur even for $N = 2$, provided that $\mathrm{sgn}\phi_{-1} \neq \mathrm{sgn}\theta$. However, $N = 2$ is too small to obtain strong asymmetry in transmission at $\mathrm{sgn}\phi_{-1} = \mathrm{sgn}\theta$; see Figs. 12(c) and 12(d). The change of $\mathrm{sgn}\phi_{-1}$ can be obtained here while unidirectionality is not kept. Hence, either tunability with switching between negative and positive deflection but without unidirectionality or strong asymmetry in transmission but without switching can be realized in this case, depending on whether the corrugated-side illumination at variable θ or both the corrugated-side and the noncorrugated-side illuminations at the proper values of θ are considered. In conclusion, it can be expected that unidirectionality and switchable sign of deflection may coexist in rather thin structures, e.g., with $N = 2$ or $N = 3$, provided that parameters are properly adjusted.

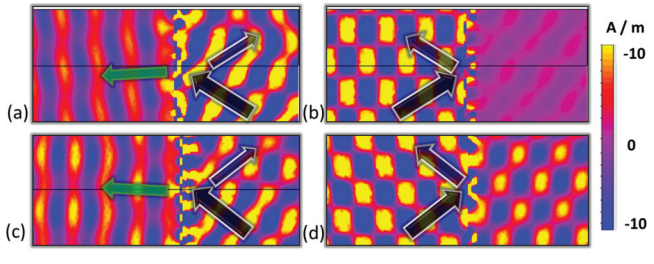

FIG. 12. (Color online) Same as Fig. 11 but for $f = 50$ GHz at (a), (b) $\theta = 32^\circ$, (c), (d) $\theta = 38^\circ$.

V. CONCLUSIONS

To summarize, we have demonstrated the diffraction-inspired unidirectional transmission arising when deflection and refraction can be tuned by varying the incidence angle. The focus has been on the general dispersion requirements, at which this mechanism can be obtained in various structures with broken symmetry, and the features of transmission for SHAs with one-side corrugations. Due to peculiar EFCs exhibited by SHAs, one might be able to achieve tunable unidirectionality in a quite compact structure. A simple geometrical consideration, which requires only information about the width of EFCs of host (meta)material and period of corrugations, enables analysis of the basic possible scenarios of tunability. Two regimes can be distinguished, in which deflection is tunable at either continuous or discrete variation of the angle of incidence. For the latter, the difference in deflection angles between negatively and positively deflected beams can reach 32° for the hybrid SHA-based structure considered in detail in this paper, while transmittance is below −10 dB. Nevertheless, a forward-to-backward transmittance contrast that exceeds 60 dB can be obtained for the ranges of both negative and positive deflection. The observed location of high transmission and stop bands and wave front behavior are in good agreement with the predictions from the dispersion based coupling analysis. Regardless of tunability, the negative deflection regime in hybrid SHA–dielectric gratings holds promise for presented subwavelength performances for unidirectional transmission. The used approach and obtained results indicate a route to high compact tunable unidirectional devices for a wide frequency range that extends at least from acoustic to terahertz frequencies. The possibility of switching from negative to positive deflection combined with directional selectivity brings up, in particular, a way of designing tunable terahertz deflectors, angular filters, and diodelike devices. Enhancing transmission in unidirectional regimes achievable in SHA-based structures will be a subject of one of our future studies.

ACKNOWLEDGMENTS

The authors are indebted to Professor Mario Sorolla for his constant support. This work was sponsored by the Spanish Government and European Union funds under contracts Consolider "Engineering Metamaterials" CSD2008-00066 and TEC2011-28664-C02-01. P.R.-U. is sponsored by the Government of Navarre via the program "Formacion de Tecnólogos" 055/01/11. M.B. is sponsored by the Spanish Government via RYC-2011-08221. M.N.-C. is supported by the Imperial College Junior Research Fellowship. The contribution of A.E.S. was partially supported by the DFG, Project No. 1409/2-2, and by the European Science Foundation under the RNP NEWFOCUS program.

*pablo.rodriguez@unavarra.es
†miguel.beruete@unavarra.es
‡m.navarro@imperial.ac.uk
§serebryannikov@tu-harburg.de

[1] M. J. Lockyear, A. P. Hibbins, K. R. White, and J. R. Sambles, Phys. Rev. E **74**, 056611 (2006).
[2] A. E. Serebryannikov, T. Magath, and K. Schuenemann, Phys. Rev. E **74**, 066607 (2006).
[3] A. Mandatori, M. Bertolotti, and C. Sibilia, J. Opt. Soc. Am. B **24**, 685 (2007).
[4] A. E. Serebryannikov and E. Ozbay, Opt. Exp. **17**, 13335 (2009).
[5] A. E. Serebryannikov, Phys. Rev. B **80**, 155117 (2009).
[6] X.-F. Li, X. Ni, L. Feng, M.-H. Lu, C. He, and Y.-F. Chen, Phys. Rev. Lett. **106**, 084301 (2011).
[7] S. Xu, C. Qui, and Z. Liu, J. Appl. Phys. **111**, 094505 (2012).
[8] X.-B. Kang, W. Tan, Z.-S. Wang, Z.-G. Wang, and H. Cheng, Chin. Phys. Lett. **27**, 074204 (2010).
[9] R. Singh, E. Plum, C. Menzel, C. Rockstuhl, A. K. Azad, R. A. Cheville, F. Lederer, W. Zhang, and N. I. Zheludev, Phys. Rev. B **80**, 153104 (2009).
[10] E. Plum, V. A. Fedotov, and N. I. Zheludev, Appl. Phys. Lett. **94**, 131901 (2009).
[11] M. Mutlu, A. E. Akosman, A. E. Serebryannikov, and E. Ozbay, Phys. Rev. Lett. **108**, 213905 (2012).
[12] A. Cicek, M. B. Yusel, O. A. Kaya, and B. Ulug, Opt. Lett. **37**, 2937 (2012).
[13] C. Lu, X. Hu, Y. Zhang, Z. Li, X. Xu, H. Yang, and Q. Gong, Appl. Phys. Lett. **99**, 051107 (2011).
[14] C. Wang, C.-Z. Zhou, and Z.-Y. Li, Opt. Express **19**, 26948 (2011).
[15] M. Beruete, A. E. Serebryannikov, V. Torres, M. Navarro-Cía, and M. Sorolla, Appl. Phys. Lett. **99**, 154101 (2011).
[16] S. Cakmakyapan, A. E. Serebryannikov, H. Caglayan, and E. Ozbay, Opt. Lett. **35**, 2597 (2010).
[17] M. Stolarek, D. Yavorskiy, R. Kotyński, C. J. Zapata-Rodríguez, J. Lusakowski, and T. Szoplik, Opt. Lett. **38**, 839 (2013).
[18] J. Xu, C. Cheng, M. Kang, Z. Zheng, Y. X. Fan, and H. T. Wan, Opt. Lett. **36**, 1905 (2011).
[19] V. G. Veselago, Sov. Phys. Usp. **10**, 50 (1968).
[20] D. R. Smith, W. J. Padilla, D. C. Vier, S. C. Nemat-Nasser, and S. Schultz, Phys. Rev. Lett. **84**, 4184 (2000).
[21] L. Solymar and E. Shamonina, *Waves in Metamaterials* (Oxford University Press, Oxford, 2009).
[22] M. Beruete, M. Sorolla, and I. Campillo, Opt. Express **14**, 5445 (2006).
[23] W. T. Lu, Y. J. Huang, P. Vodo, R. K. Banyal, C. H. Perry, and S. Sridhar, Opt. Express **15**, 9166 (2007).
[24] S. Foteinopoulou and C. M. Soukoulis, Phys. Rev. B **72**, 165112 (2005).
[25] J. H. Wu, L. K. Ang, A. Q. Liu, H. G. Teo, and C. Lu, J. Opt. Soc. Am B **22**, 1770 (2005).
[26] J. Bucay, E. Roussel, J. O. Vasseur, P. A. Deymier, A.-C. Hladky-Hennion, Y. Pennec, K. Muralidharan, B. Djafari-Rouhani, and B. Dubus, Phys. Rev. B **79**, 214305 (2009).
[27] A. E. Serebryannikov, A. Y. Petrov, and E. Ozbay, Appl. Phys. Lett. **94**, 181101 (2009).
[28] The term *host material* is assumed here to be assignable to both MMs and photonic crystals, i.e., periodic structures with a rather arbitrary period, which can be characterized in terms of FB modes. It is assumed that higher diffraction orders cannot appear due to the intrinsic periodicity, at least within the considered range of parameter variation. Thus, the noncorrugated interface of the slab of a host material cannot itself create a higher diffraction order that may propagate in air.
[29] R. Petit, editor, *Electromagnetic Theory of Gratings* (Springer, Berlin, 1980).
[30] In the case of a square or rectangular lattice, this means that EFCs are located around the Γ point of the first irreducible Brillouin zone.
[31] Strictly speaking, circular EFCs being narrower than in air correspond to materials with the effective index of refraction $|n_{\text{eff}}| < 1$, provided that homogenization is applicable. Such EFCs are also typical for some of Floquet-Bloch modes in photonic crystals.
[32] M. Beruete, I. Campillo, M. Navarro-Cía, F. Falcone, and M. Ayza, IEEE Trans. Antennas Propag **55**, 1514 (2007).
[33] D. R. Smith and D. Schurig, Phys. Rev. Lett. **90**, 077405 (2003).
[34] M. Beruete, M. Navarro-Cía, and M. Sorolla, New J. Phys. **12**, 063037 (2010).
[35] S. Cherukulappurath, D. Heinis, J. Cesario, N. F. van Hulst, S. Enoch, and R. Quidant, Opt. Exp. **17**, 23772 (2009).